Chemical Vapor Deposition

DOI: 10.1002/cvde.200606566

Full Paper

Visualization of Vortex Flow Patterns with a Uniformly Perforated Showerhead in a Model Lamp Heat, Single-Wafer Thermal Processor

By *Tsung Chieh Cheng*,* *Tsing Fa Lin*, *Jung Yen Yang*, and *Sheng-Rui Jian*

Following the rapid progress in the growth of semiconductor thin crystal films, rapid thermal (RT) CVD not only allows for minimization of processing and cycle time, but also enables a significant reduction in the thermal budget. The flow recirculation in the processing chamber driven by the large buoyancy resulting from the temperature differences between the wafer and input gases is known to produce detrimental effects on the film properties. In this study, the proposed 8″ rapid thermal processor (RTP) with a showerhead inlet contains three basic types of flow patterns (plug, mixed, and buoyancy-induced flow). The physical parameters, gas flow rate, and pressure of processing chamber are investigated in detail.

Keywords: Buoyancy induced flow, Mixed flow, Plug flow, Rapid thermal process

1. Introduction

The performance of a growth apparatus depends strongly on physical and chemical aspects such as the fluid dynamics and deposition chemistry. For a basic deposition apparatus, the vortex flow induced by multiple jets impinging on a heated disk in a confined cylindrical chamber is frequently encountered in various technological processes such as cooling of microelectronic equipment,[1] growth of thin crystal films,[2–4] and fabrication of ultra large scale integrated (ULSI) circuits.[5] In a previous study, an experimental flow visualization, conducted for two impinging jets,[6] showed that two vortices are generated in the space between the main vortexes and the bottom flat plate. Elbanna and Sabbagh[7] indicated that increasing the distance between the exit plane of the jets and the ground plate caused a stagnation pressure to develop in the upwash formation region. Moustafa and Rathakrishnan[8] studied the flow field of multijets with square configuration, and showed that the mean velocity profile as well as the mean velocity decay had fairly weak dependence on the pressure ratio. Therefore, the turbulent flow field associated with co-flowing jets and jet arrays was classified into two categories based on their formation and the regions where they resided: (1) large scale structures developed by impinging; and (2) shear layer structures induced by both the shear layer instability and the return flow.[9] For a large number of planar coflowing interacting jets,[10] there is a merging length where the jet diameter reaches the size of the jet spacing. At this merging point the mean velocity appears essentially uniform. Furthermore, the empirical equations for predicting the heat and mass transfer coefficients for multiple impinging jets and the hot-wall chamber were proposed by Martin[11] and by Hu and Hüttinger.[12]

Fluid flow and heat transfer in various types of CVD reactors[13] and RTP processors have been the focus of many investigations. Özturk et al.[14] proposed that three challenging issues were needed to be addressed: (1) to obtain a uniform thin film, the thickness of the velocity, temperature, and concentration boundary layers[15] over the wafer must be uniform; (2) the wafer must be at a uniform temperature to reduce the thermal stresses; and (3) for interface abruptness, the gas flow in the reactor must be free of any vortices to minimize gas residence time. Therefore, the absence of gas flow recirculation is important in the RT CVD chamber. Depending on the flow and thermal conditions, there are three fundamental types of flow regimes in a vertical reactor,[16] namely plug flow (force-convection dominated flow),[17] buoyancy-induced flow, and rotation-induced flow.[18] The plug flow pattern, in turn, produces a uniform boundary layer flowing over the wafer and stabi-

[*] Prof. T. C. Cheng,[+] Dr. J. Y. Yang
National Nano Device Laboratories, Nanometrology
Hsinchu 30078, Taiwan (R.O.C.)
E-mail: tcchengme@cc.kuas.edu.tw
Prof. T. F. Lin
Department of Mechanical Engineering, National Chiao Tung University
Hsinchu, 30010, Taiwan (R.O.C.)
Prof. S.-R. Jian[++]
Department of Electrophysics, National Chiao Tung University
Hsinchu 30010, Taiwan (R.O.C.)

[+] Present address: Department of Mechanical Engineering, National Kaohsiung University of Applied Sciences, Kaohsiung 80778, Taiwan ROC.

[++] Present address: Department of Materials Sciences and Engineering, I-Shou University, Kaohsiung 80840 Taiwan ROC.

lizes the flow as well. Thus, plug flow is good for many thin film growth applications. Moreover, as the gas enters the reactor through a single-inlet tube, the recirculation cell could be eliminated by increasing the inlet gas flow rate.[19] For low pressure CVD in a single-wafer reactor, Kleijn et al.[20] reach a similar conclusion in their numerical computation of the gas flow. Patnaik et al.[21] also showed that operating at a pressure of 0.2 atm gave good epilayer uniformity and interface abruptness for GaAs-AlGaAs growth in metal-organic (MO)CVD. Besides, decreasing the nozzle-plate spacing, accelerating the fluid flow, and significantly increasing the local air turbulence will create a nonuniformity in the flow over the wafer.[22] Furthermore, several simulations of the transport phenomena in the CVD reactor have been studied with various susceptor rotation rates.[23,24] The results indicated that the uniformity near the susceptor edge can still be tuned by the susceptor rotation.[25] Meanwhile, a stable flow can be achieved if the mixed convection parameter is less than 2.[26]

The above literature reviews clearly reveals that the performance of thin film growth depends on the mixed flow characteristics in the chamber, and the ranges of the important relevant dimensionless groups Re and Ra are 0.1–100 and $1–10^5$, respectively.[27] However, there is no direct experimental evidence for these vortex flow patterns. In this study, an experimental system is established to observe the vortex flow patterns in this confined, uniformly perforated showerhead (impinging multijets) flow. Attention is focused on how the jet flow rate, temperature difference between the plate and jet, and chamber pressure affect the vortex flow patterns.

2. Results

2.1. Typical Flow Patterns

At first, the typical flow patterns observed in the processing chamber at steady or statistically stable state can be broadly classified into three types. The selected flow photos from the side view and the corresponding schematically sketched flow patterns are also illustrated in Figure 1. These include the plug flow, buoyancy-induced flow, and mixed buoyancy-induced and plug flow, depending on the buoyancy-to-inertia ratio Gr/Re^2 in the flow. Some important flow characteristics associated with these flow patterns are briefly described below.

2.1.1. Plug Flow

The plug flow shown in Figure 1a, which prevails at a low buoyancy-to-inertia ratio, is like a plane stagnation flow in a confined space. More specifically, the air flow moving across the showerhead travels nearly vertically downward into the processing chamber. As the flow approaches the wafer (copper plate), it is deflected by the plate to move radially outwards. The flow then moves downwards after leaving the edge of the wafer along the sidewall of the reactor chamber. Finally, the flow leaves the processor from the exhaust ports. Note that there exists a weak circular roll near the upper corner of the processing chamber, though the entire flow is axisymmetric. Obviously the plug flow is dominated by the inertia force and no flow recirculation appears above the copper plate.

2.1.2. Buoyancy-Induced Flow

When the buoyancy-to-inertia ratio is high, a strong and large circular vortex roll is induced by the heated copper plate (Fig. 1b), which occupies nearly the entire processing chamber. Hence the inlet flow from the mixing chamber is immediately deflected by this roll to move along the showerhead and the lateral wall of the processor. Obviously, the flow is dominated by the buoyancy force,[17] and the vortex roll is characterized by the ascending flow in the center region of the chamber and the descending flow near the chamber side. In addition, the flow can be axisymmetric.

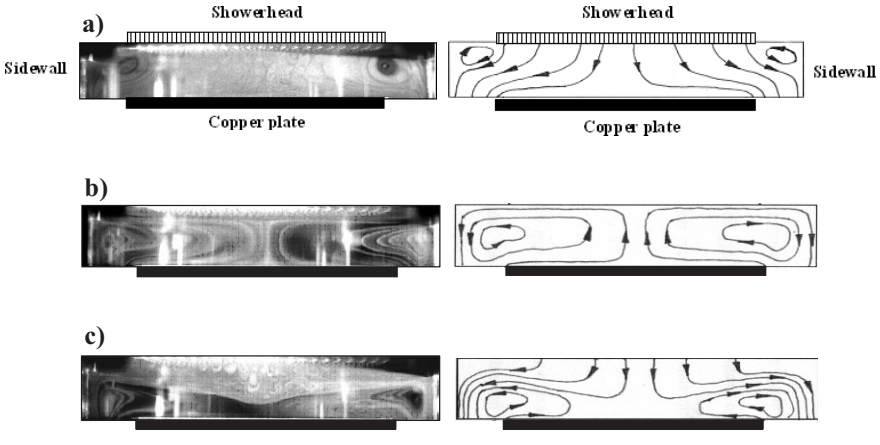

Fig. 1. Flow photos and the corresponding schematically sketched typical long time gas flow patterns in the processing chamber with uniformly perforated showerhead. a) plug flow, b) buoyancy-induced flow, and c) mixed plug and buoyancy-induced flow.

2.1.3. Mixed Plug and Buoyancy-Induced Flow

A mixed plug and buoyancy induced flow results at an intermediate buoyancy-to-inertia ratio (Fig. 1c). The flow is simultaneously driven by the inertia and buoyancy. Specifically, a weaker and smaller circular vortex roll appears near the outer zone of the processing chamber, and the inlet flow from the mixing chamber is deflected to move outwards by this roll half way before it reaches the wafer. Then the deflected flow turns to trav-

el downward as it hits the sidewall of the processor. The flow again can be axisymmetric and similar simulation results were also indicated by Houtman et al.[28] It should be noticed that no circular roll is induced in the upper corner of the processing chamber in this case.

2.2. Effects of Gas Flow Rate

The air flow rate across the showerhead affects the long-time gas flow pattern in the processing chamber, as shown manifested in Figure 2. Note that at given ΔT and P, the increase in the flow rate raises the flow inertia, and so the buoyancy-to-inertia ratio becomes lower. Thus, at high Q, the resulting flow tends to be dominated by the inertia force. As shown in Figure 2, a typical plug flow prevails in the chamber at the flow rate $Q = 18$ slpm ($\mathrm{Re} = 117.5$) for the case with $\Delta T = 10\,^{\circ}\mathrm{C}$ and $P = 600$ Torr ($\mathrm{Ra} = 4.43 \times 10^4$). Specially, the forced air flow from the mixing chamber moves downward to the copper plate and then over the entire plate surface. There is no buoyancy-induced flow recirculation above the wafer. However, when the flow rate decreases slightly, a circular vortex roll appears near the wafer edge and it becomes larger for a lower value of Q (Figs. 2f and 2 g). Then the mixed plug and buoyancy-induced flow results for an even lower value of Q, at which both the buoyancy and inertia play important roles (Figs. 2d) and 2e)). For a further reduction in the gas flow rate, the buoyancy driven vortex roll gets stronger and larger (Figs. 2c) and 2d)) with the accompanying decay of the weak roll in the upper corner of the processing chamber. As the value of Q is lowered even further to 2 slpm, the entire flow is dominated by the buoyancy driven vortex roll (Figs. 2a and 2b).

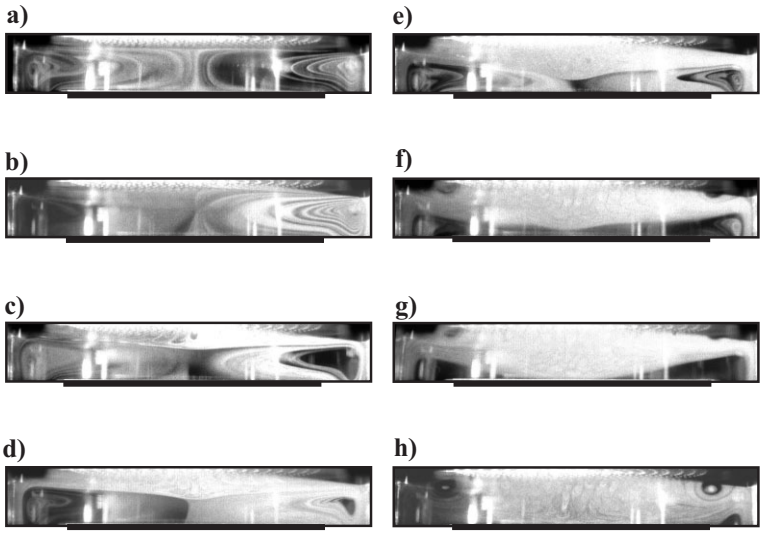

Fig. 2. Steady flow patterns viewed from the chamber side for various values of flow rate, Q, at $P = 600$ Torr and $\Delta T = 10\,^{\circ}\mathrm{C}$. ($\mathrm{Ra} = 4.43 \times 10^4$). a) 4 slpm ($\mathrm{Re} = 26.1$), b) 6 slpm ($\mathrm{Re} = 39.2$), c) 8 slpm ($\mathrm{Re} = 52.2$), d) 10 slpm ($\mathrm{Re} = 65.3$), e) 12 slpm ($\mathrm{Re} = 78.3$), f) 14 slpm ($\mathrm{Re} = 91.4$), g) 16 slpm ($\mathrm{Re} = 104.4$), and h) 18 slpm ($\mathrm{Re} = 117.5$).

2.3. Effects of Wafer/Inlet Air Temperature Difference

The effects on the recirculating flow in the processing chamber of the temperature difference between the copper plate and the inlet air drawn from the ambient atmosphere into the processor are presented in Figure 3 for ΔT ranging from 0 °C to 20 °C. The results in Figure 3 for the chamber pressure $P = 600$ Torr and gas flow rate $Q = 12$ slpm ($\mathrm{Re} = 78.3$) indicate that, except for $\Delta T = 0\,^{\circ}\mathrm{C}$ ($\mathrm{Ra} = 0$), the flow is dominated by the mixed vortex roll at this low gas flow rate. For $\Delta T = 0\,^{\circ}\mathrm{C}$, no buoyancy effect exists and the flow in the processing chamber is completely driven by the inertia force of the inlet flow. Please note that the effects of the temperature difference on the gas flow pattern are somewhat different at a higher value of Q. According to the results in Figure 3 for $Q = 12$ slpm, we have mixed flow structure for all $\Delta T \geq 5\,^{\circ}\mathrm{C}$. Specifically, the flow in the chamber can be divided into two zones, one on top of the other. In the upper zone plug flow prevails. Buoyancy-induced flow dominates in the lower zone. As temperature difference increases, the buoyancy-induced roll is stronger and larger, and the plug flow zone is correspondingly small-

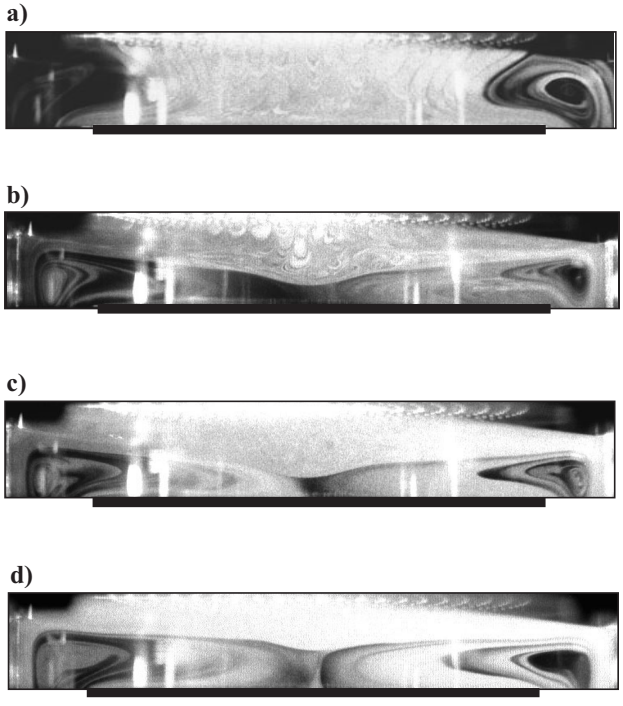

Fig. 3. Steady flow patterns viewed from the chamber side for various values of inlet-to-susceptor temperature difference, ΔT, at $P = 600$ Torr and $Q = 12$ slpm. ($\mathrm{Re} = 78.3$). a) 0 °C ($\mathrm{Ra} = 0$), b) 5 °C ($\mathrm{Ra} = 2.38 \times 10^4$), c) 10 °C ($\mathrm{Ra} = 4.43 \times 10^4$), and d) 15 °C ($\mathrm{Ra} = 6.18 \times 10^4$).

er (Figs. 3b–3d). It is interesting that the buoyancy force is increasing with increasing temperature difference. This rise in temperature difference also causes buoyancy-induced recirculation flow to become stronger and compresses the plug flow.

2.4. Effects of Chamber Pressure

The operating pressure, P, in the processing chamber is expected to significantly affect the buoyancy-driven recirculating flow in the chamber. This can be attributed to the fact that the Re of the inlet flow across the showerhead is independent of P for fixed inlet gas flow rate, since the gas velocity varies inversely with P while the gas in density is directly proportional to P, and the dynamic viscosity of the gas is little affected by the pressure. Moreover, at a given mass flow rate of air injected into the processor, and given imposed temperature difference between the inlet air and copper plate, the Rayleigh number of the gas flow in the chamber is proportional to the square of the gas pressure.[16] Thus, lowering the chamber pressure can effectively reduce the natural convection effects and hence decrease the strength of the buoyancy-driven recirculation flow in the chamber. This can be clearly seen from the results in Figure 4. At a chamber pressure of 760 Torr, buoyancy-induced flow dominates in the entire chamber at fixed $\Delta T = 5$ °C and $Q = 4$ slpm, as illustrated in Figure 4d) ($Re = 26.1$ and $Ra = 3.83 \times 10^4$). For a small reduction of P to 450 Torr, the buoyancy-induced flow weakens substantially, and the plug flow appears in the upper zone near the showerhead (Fig. 4b)) ($Re = 26.1$ and $Ra = 1.34 \times 10^4$). Notably, at $P = 300$ Torr, the buoyancy-induced vortex roll nearly disappears (Fig. 4a)) ($Re = 26.1$ and $Ra = 5.96 \times 10^3$). Thus, we observe plug flow in the outermost region of the chamber. Similar trend is noted for other values of Q and ΔT. For high values of Q and ΔT, the shrinkage of the buoyancy-driven roll is rather pronounced for decreasing pressure.

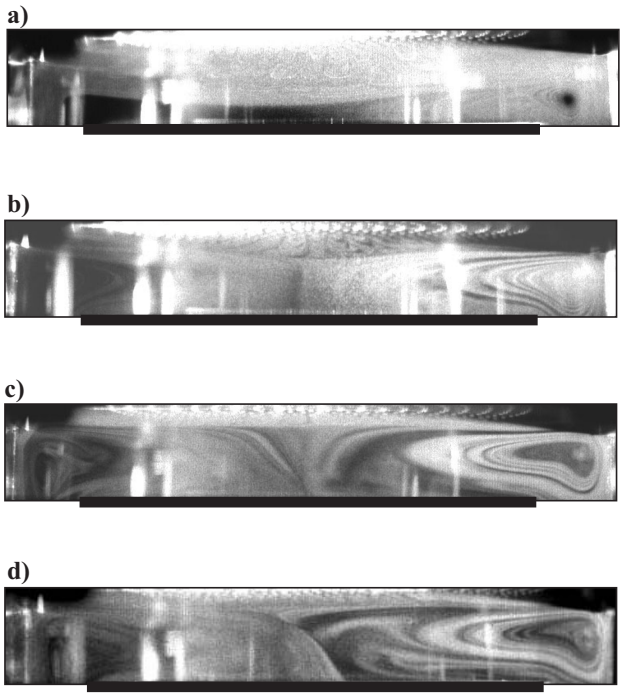

Fig. 4. Steady flow patterns viewed from the chamber side for various values of chamber pressure, P, at $\Delta T = 5$ °C and $Q = 4$ slpm. ($Re = 26.1$). a) 300 Torr ($Ra = 5.96 \times 10^3$), b) 450 Torr ($Ra = 1.34 \times 10^4$), c) 600 Torr ($Ra = 2.39 \times 10^4$), and d) 760 Torr ($Ra = 3.83 \times 10^4$).

2.5. The Flow Regime Map

Base on the present data, a flow regime map in terms of Ra vs. Re delineating the three distinct gas flow patterns in the processing chamber is provided in Figure 5. The results suggest that under a pressure of

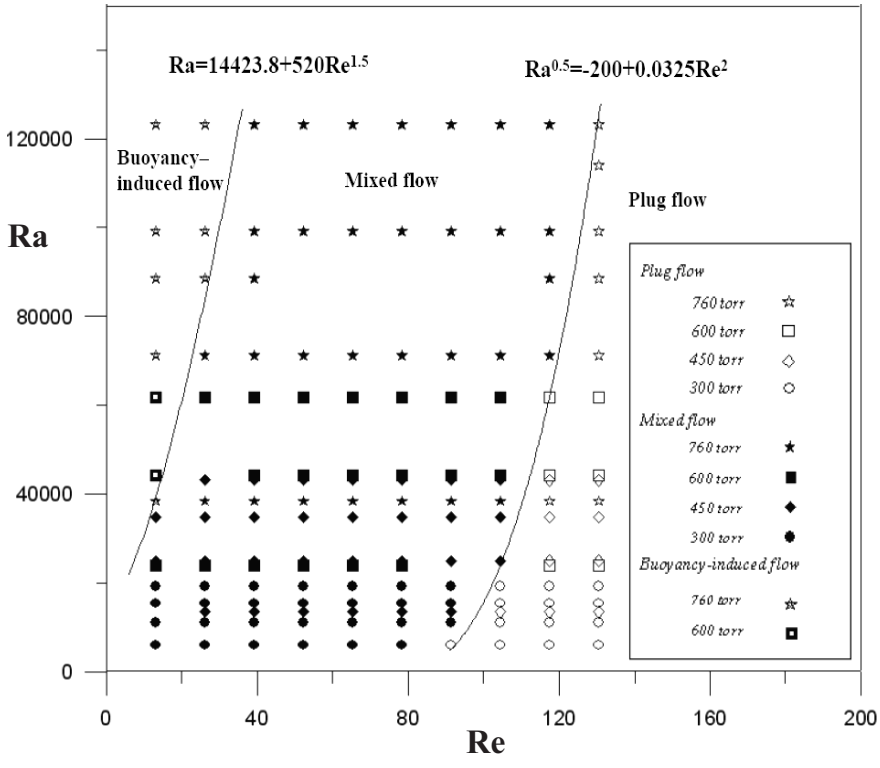

Fig. 5. The flow regime map for a uniformly perforated showerhead.

760 Torr, the buoyancy force for all cases is high, and the buoyancy-induced vortex low prevails at very low Reynolds number. Under lower pressure, the buoyancy is lower and the mixed flow pattern appears because of the simultaneous importance of the buoyancy and inertia force. If we reduce the Rayleigh number by lowering the pressure further, or increase the Reynolds number, the inertia force of the inlet gas flow is high and the plug flow dominates in the chamber. As shown in Figure 5, the boundary between the mixed and plug flow can be correlated as shown in Equation 1.

$$Ra^{0.5} = -200.0 + 0.00325\ Re^2 \quad (1)$$

The boundary between the buoyancy-induced flow and mixed flow can be represented by Equation 2.

$$Ra = 14423.8 + 520.0\ Re^{1.5} \quad (2)$$

It is interesting to understand how the Reynolds and Rayleigh numbers affect the vertically downward moving distance of the inlet gas flow across the showerhead for the mixed flow pattern. In each photo, the longest distance (L_p) from the showerhead to the border between the buoyancy-induced and the plug flows is measured. Based on these data, the longest moving distance of the plug flow can be correlated as shown in Equation 3.

$$L_p/H = -1.69 + 0.015\ Re + 473.16\ \ln(Ra)/Ra \quad (3)$$

The above correlation and the data collected are compared in Figure 6. The results indicate that increasing the Reynolds number and/or decreasing the Rayleigh number will enlarge the plug flow zone.

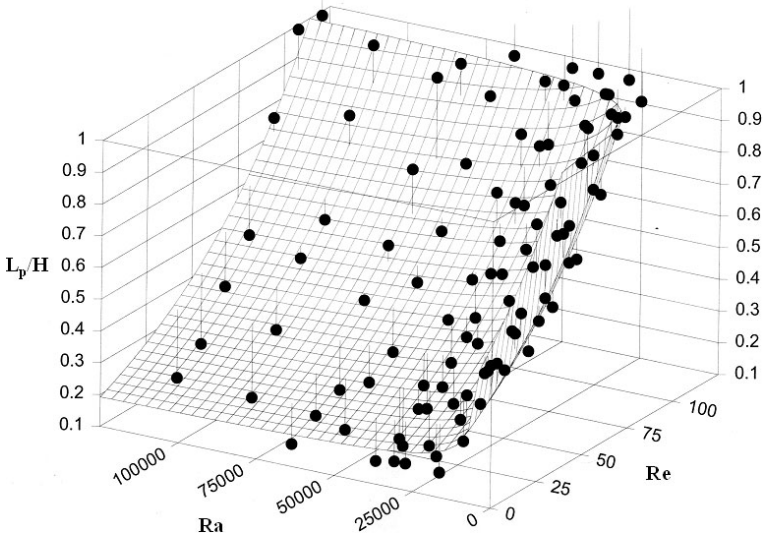

Fig. 6. Comparison of the correlation of the dimensionless moving distance L_p/H of the plug flow with measured data. (● denotes the data and the 3-D surface represents the equation $\ln(L_p/H) = -1.69 + 0.015\ Re + 473.16\ \ln(Ra)/Ra$.

3. Concluding Remarks

The gas flow patterns revealed from the flow visualization for the uniformly perforated showerhead have been successfully examined in this paper. The flow in the processing chamber can be classified into three types: plug flow, buoyancy-induced flow, and mixed buoyancy-induced and plug flow. These flow characteristics can be briefly summarized in the following.

1. A rise in the gas flow rate compresses the buoyancy-induced vortex roll and enlarges the plug flow zone.
2. Reducing the chamber pressure significantly decreases the Rayleigh number and can suppress the buoyancy-induced flow. This reducing pressure even eliminates the buoyancy driven vortex flow when the pressure is low enough.
3. Correlating equations are provided to delineate various recirculating flow patterns and the moving distance of the plug flow for the mixed flow pattern.

It should be mentioned here that what is required is not only the plug flow in the processing chamber but also uniform velocity and temperature boundary layers over the wafer. In these experiments, the basic concepts for the design of the practical RTCVD processor have been successfully provided.

4. Experimental

The experimental system is schematically illustrated in Figure 7. It has been used to investigate the mixed convective vortex flow patterns, resulting from the showerhead, impinging onto a heated disk in a cylindrical chamber. This system simulates the flow in a single-wafer RTP processor. It consists of six major parts – the processing chamber, temperature measurement and data acquisition unit, heating lamp unit, gas injection unit, vacuum unit, and control unit. In these experiments, the processing chamber is cylindrical and has a diameter of 30 cm. Its side wall is made of quartz glass, 6 mm thick, to enable observation of the flow patterns in the chamber. The entire chamber is insulated with a superlon insulator, 10 cm thick. The insulator is only opened during the flow visualization experiment. A circular copper plate, 1 cm thick, having a diameter of 20 cm, is used to simulate an 8-inch wafer. Eight T-type thermocouples are stuck on the copper plate at selected locations to measure the temperature variations over the copper plate. To simulate the flow in a RTP system, the copper plate is heated by lamps. The lamp-heating unit consists of thirteen 410 W, 82 V, OSRAM tungsten-halogen lamps (with reflector), which are arranged into an inner ring of four lamps and an outer ring of nine lamps. The input power to each lamp zone can be automatically adjusted in real time using two variable resistance circuits to optimize the temperature uniformity of the wafer. The results indicate that the maximum temperature nonuniformity across the wafer deviating from the average copper plate temperature is about ±0.3 °C.

In the present study, the system pressure of the chamber is maintained at the required level by adjusting the flow rate of the vacuum pump. For each case the experiment starts with the air at room temperature, T_a, compressed first into a smoke generator through the connection pipe and then injected into the processing chamber. Flow visualization is conducted when the flow has already reached steady state, or a statistically stable state at which all the initial transients die out, by using a vertical plane light sheet to shine through the flow field containing tiny incense particles. The thin plane light sheet is produced by two razor blades and a YOKOGAWA xenon slide

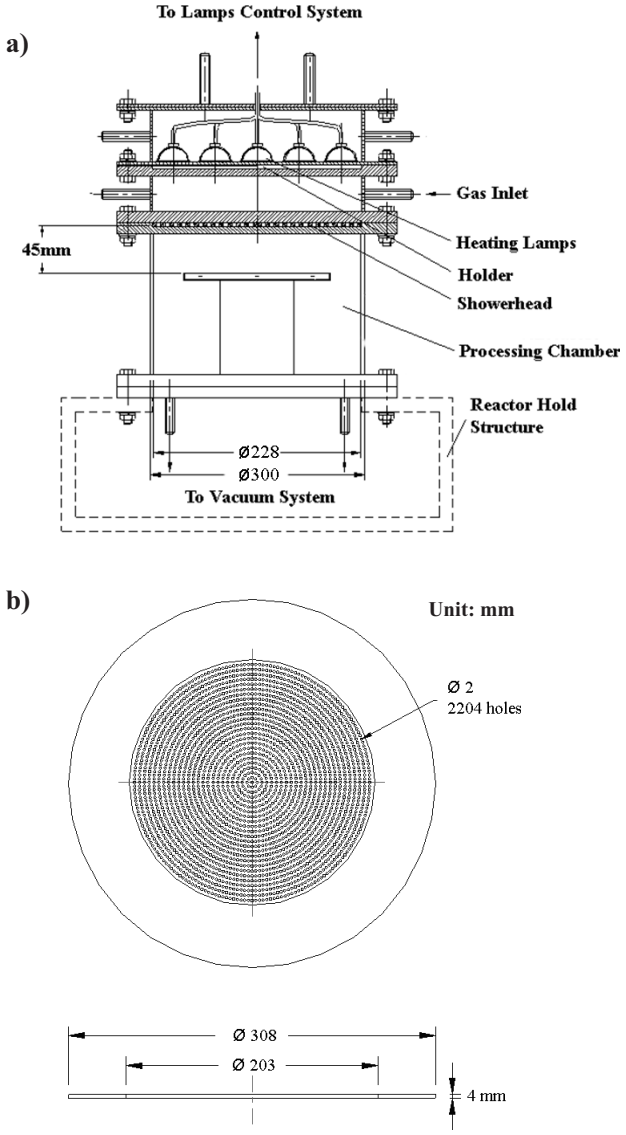

Fig. 7. a) The RTP chamber configuration. b)The showerhead with uniformly perforated holes.

projector. A Nikon FM2 camera with a maximum diaphragm of 1.4 and suitable exposure time (varying from 1/60 – 1/4 s) is used to picture the flow patterns from the chamber side. Also, a digital video camera (Sony PC-100) takes consecutive pictures of the time-dependent flow patterns. Moreover, an uncertainty analysis based on the procedures proposed by Kline and McClintock [29] was carried out to estimate the uncertainty levels in the experiment. The results from this uncertainty analysis are summarized in Table 1. The side-view flow photos taken from the model RTP processor with the showerhead having 2401 holes of uniform size (holes diameter is 2mm) are also examined. In the experiment, the gas flow rate (Q_i) is varied from 2 to 20 slpm, temperature difference (ΔT) is varied from 0 to 20 °C, and the chamber pressure (P) is varied from 300 to 760 Torr. The dimensionless groups associated with the flow considered here are the Reynolds number (Re) and Rayleigh number (Ra). The gas flow patterns in the processing chamber obtained in this study are presented here with the showerhead-to-wafer distance fixed at $H = 4.5$ cm. Particular attention is paid to the delineation of various vortex flow patterns driven by the combined inertia and buoyancy forces in the processing chamber.

Received: December 18, 2006
Revised: May 11, 2007

Table 1. Summary of uncertainty analysis.

Parameters	Uncertainty
Diameter of processing chamber, D	± 0.00005 m
Wafer diameter, D_{wf}	± 0.00005 m
Distance of showerhead to wafer, H	± 0.00005 m
Chamber pressure, P	± 1 Torr
Temperature of wafer, T_{wf}	± 0.3 °C
Ambient temperature, T	± 0.3 °C
Temperature difference between the wafer and showerhead, ΔT	± 0.4 °C
Dynamic viscosity of fluid , μ [Nm s^{-2}]	± 0.05 %
Kinematic viscosity, v [m^2 s^{-1}]	± 0.07 %
Fluid speed, V [m s^{-1}]	± 1.4 %
Mass flow rate, Q [L min^{-1}]	± 1.5 %
Rayleigh number, Ra = $\beta g \Delta T H^3/\alpha v$	± 10.6 %
Reynolds number, Re = VD/v	± 2.4 %

[1] S. Polat, B. Huang, A. S. Mujumdar, W. J. M. Douglas, *Annu. Rev. Numer. Fluid Mech. Heat Transfer*, Hemisphere, Washington, D. C. **1989**, *2*, 157.
[2] G. B. Stringfellow, *Organometallic Vapor Phase Epitaxy*, Academic Press, San Diego **1989**.
[3] R. Müller, U. Künecke, D. Queren, S. A. Sakwe, P. Wellmann, *Chem. Vap. Deposition*, **2006**, *12*, 557.
[4] C. R. Kleijn, K. J. Kuijlars, M. Okkerse, H. van Santeen, H. E. A. van den Akker, *J. Phys. IV* **1999**, (Pr8) *9*, 117.
[5] S. A. Campbell, *The Science and Engineering of Microelectronic Fabrication*, Oxford University Press, New York **1996**.
[6] C. Carcasci, *Int. J. Therm. Sci.* **1999**, *38*, 808.
[7] H. Elbanna, J. A. Sabbagh, *AIAA J.* **1989**, *27*, 420.
[8] G. H. Moustafa, E. Rathakrishnan, *AIAA J.* **1993**, *31*, 1189.
[9] S. C. Arjocu, J. A. Liburdy, *J. Heat Transfer* **1999**, *121*, 384.
[10] E. Villermaux, E. J. Hopfinger, *J. Fluid Mech.* **1994**, *263*, 63.
[11] H. Martin, *Advances in Heat Transfer*, Academic Press, San Diego **1997**, p. 1.
[12] Z. J. Hu, K. J. Hüttinger, *Chem. Vap. Deposition* **2000**, *6*, 77.
[13] L. Kadinski, V. Merai, A. Parekh, J. Ramer, E. A. Armour, R. Stall, A. Gurary, A. Galyukov, Y. Makarov, *J. Cryst. Growth* **2004**, *261*, 175.
[14] M. C. Özturk, F. Y. Sorrell, J. J. Wortman, F. S. Johnson, D. T. Grider, *IEEE Trans. Semicond. Manuf.* **1991**, *4*, 155.
[15] H. Schlichting, *Boundary Layer Theory*, McGraw-Hill, New York **1979**.
[16] C. R. Biber, C. A. Wang, S. Motakef, *J. Cryst. Growth* **1992**, *123*, 545.
[17] H. V. Santen, C. R. Kleijn, H. E. A van Den Akker. *Int. J. Heat Mass Transfer* **2001**, *44*, 659.
[18] C. Weber, V. C. Opdrop, *J. Appl. Phys.* **1990**, *67*, 109.
[19] D. I. Fotiads, S. Kieda, K. F. Jensen, *J. Cryst. Growth* **1990**, *102*, 441.
[20] C. R. Kleijn, T. H. V. D. Meer, C. J. Hoogendoorn, *J. Electrochem. Soc.* **1989**, *136*, 3423.
[21] S. Patnaik, R. A. Brown, C. A. Wang, *J. Cryst. Growth* **1989**, *96*, 153.
[22] D. Lytle, B. W. Webb, *Int. J. Heat Mass Transfer* **1994**, *37*, 1687.
[23] G. H. Evans, R. Greif, *Numer. Heat Transfer* **1988**, *14*, 373.
[24] R. P. Pawloswki, A. G. Salinger, L. A. Romero, J. N. Shadid, *J. Phys. IV* **2001**, (Pr3) *11*, 197.
[25] Y. J. Kim, J. H. Boo, B. Hong, *Surf. Coat. Technol.* **2005**, *193*, 88.
[26] W. G. Breiland, G. H. Evans, *J. Electrochem. Soc.* **1991**, *138*, 1806.
[27] M. Masi, M. Di Stanislao, A. Veneroni, *Prog. Cryst. Growth Charact. Mater.* **2003**, *47*, 239
[28] C. Houtman, D. B. Graves, K. F. Jensen, *J. Electrochem. Soc.* **1986**, *133*, 961.
[29] S. J. Kline, F. A. McClintock, *Mech. Eng.* **1953**, *75*, 3.

